

Rescaling of spatio-temporal sensing in eukaryotic chemotaxis

Keita Kamino, ^{1¶*} Yohei Kondo, ^{2¶*}

¹FOM Institute AMOLF, Amsterdam, Netherlands, ²Graduated school of Informatics, Kyoto University, Kyoto, Japan,

*Corresponding author

Email:

k.kamino@amolf.nl (KK)

ykondo@sys.i.kyoto-u.ac.jp (YK)

[¶]These authors contributed equally to this work.

Abstract

Eukaryotic cells can detect the direction of a chemoattractant gradient precisely by generating intracellular gradients of signaling molecules that mirror the extracellular gradient – an ability called directional sensing. Quantitative experiments have revealed two characteristic input-output relations of the system: First, in spatially-graded stimuli, the internal gradients of the signaling molecules at steady state reflect the relative steepness—rather than the absolute concentration—of the chemoattractant along the cell body. Second, upon a spatially homogeneous temporal increase in the chemoattractant concentration, the signaling molecule is transiently activated such that the response magnitude is determined by the ratio of the change in the input stimuli before and after the increase. However, the underlying mechanisms that endow the system with these response properties remain elusive. Here, by adopting a widely used modeling framework of directional sensing, i.e., local excitation and global inhibition (LEGI), we propose the hypothesis that the two scaling behaviors stem from a single design principle, namely, invariance of the governing equations to a scale transformation of the input level. Analyses of the LEGI-based model identify two different types of scale invariance, each of which is responsible for the two response properties. Our hypothesis leads to an experimentally testable prediction that a system with both types of invariance detects the relative steepness even in spatio-temporal gradient stimuli such as waves. Furthermore, we show that such behavior is independent of specific network topologies as long as the scale invariance holds, demonstrating the generic relationship between the scale invariance and the response properties.

Introduction

Many eukaryotic cells exhibit chemotaxis – the ability to sense and move up or down spatial gradients of chemicals. Chemotaxis underlies many biological phenomena such as cancer metastasis, immune response, wound healing and embryonic development (1–3). In a chemoattractant gradient, cells are constantly monitoring the direction of the gradient by means of chemical reactions on and within the cell membrane that create gradients of signaling molecules in the cytosol with the same orientation as the external stimulus. This mechanism, functioning like an internal chemical compass, is referred to as directional sensing. In spite of extensive characterization of proteins and small molecules that constitute the parts of this chemical system (3), there is a shortage of general design principles that characterize the flexible and dynamic behavior of the chemical network at a systems level.

The signal transduction events in eukaryotic chemotaxis have been most extensively studied in *Dictyostelium* and neutrophils (4). Although specific molecular species of chemoattractant depends on the type of cells, many of identified molecular components are conserved across cell types (3). Chemotactic response is initiated by binding of chemoattractants to G-protein coupled receptors (GPCRs) on the cell membrane (3–5). The binding causes dissociation of the G-protein α and $\beta\gamma$ subunits within the cell membrane (6, 7). Studies suggest that the $\beta\gamma$ subunit mediates activation of downstream effectors such as Ras proteins (8). The switching of the activity of Ras proteins are regulated by multiple guanine nucleotide exchange factors (GEFs) and GTPase-activating proteins (GAPs). The former transform Ras proteins from inactive guanosine diphosphate (GDP)-bound form to active guanosine triphosphate (GTP)-

bound form and the latter works in the opposite direction (9). The GTP-bound Ras proteins activate phosphoinositide 3-kinase (PI3K) that synthesizes phosphatidylinositol 3,4,5-triphosphate (PIP₃) from phosphatidylinositol 4,5-bisphosphate (PIP₂). Accumulation of PIP₃ on the membrane recruits multiple PH domain-containing proteins to the membranes such as Cytocolic Regulator of Adenylyl Cyclase (CRAC), protein kinase BA and PH domain protein A (PhdA), which are involved in the force-generating process of actin polymerization, or pseudopod extension (3).

Activated Ras proteins, PI3K and PIP₃ can be seen as outputs of the directional sensing system in that the molecules exhibit clear localization to the site of highest concentration of chemoattractant (10–14). The spatial profile of these molecules have been shown to be steeper than that of a gradient of chemoattractant, i.e., the directional signal is amplified (15), whereas the upstream signal, dissociation of the G-protein α and $\beta\gamma$ subunits, simply mirrors the local concentration of chemoattractant without significant amplification (16). Furthermore, the outputs of the directional sensing system are separable from the motility of cells because even an immobilized cell by an inhibitor of actin polymerization shows localization of the signaling molecules (3, 11, 14, 15). Importantly, even though the localization of the signaling molecules is persistent as long as a gradient of chemoattractant exists, the same molecules accumulate on the cell membrane only transiently upon elevation of the chemoattractant concentration if the stimulus is spatially homogeneous (12, 17). Such intriguing response properties have posed a challenge to understanding the mechanisms underlying the behavior of the system.

A conceptual scheme called local excitation and global inhibition (LEGI) has been proposed to explain directional sensing in such systems (11). The basic idea of the LEGI hypothesis is that the binding of a chemoattractant molecule to the receptor on the cell membrane elicits two counteracting processes, i.e., excitation and inhibition of the output signal of the directional sensing module. Both the excitation and inhibition processes are persistent as long as the stimulation is around, but they operate in different spatio-temporal scales. The excitation process is fast in its response time but has a shorter range of action in space, so the degree of excitation at each site on the membrane reflects the local concentration of chemoattractant. On the other hand, the inhibition process is slow but has a longer range of action in space, so the local level of inhibition reflects mean concentration of chemoattractant along the cell periphery. Upon spatially uniform stimuli, the fast nature of excitation causes transient increase in the output level but the slow inhibition process suppresses it with increasing strength. Eventually the output level goes back to the pre-stimulus level and adapts at a steady state. In spatially-graded stimuli, however, the degree of excitation differs along the gradient of the stimuli whereas the level of inhibition is nearly uniform. As a result, excitation exceeds inhibition at the site of higher concentration of chemoattractant and the opposite occurs at the lower side and therefore the system establishes a persistent graded response. Mathematical models have been proposed implementing the mechanism with various assumptions on the detailed structure (1, 14, 17–21). Although experimental evidence for the LEGI mechanism is still limited, these models have proved successful in a qualitative explanation of experimentally-characterized behaviors of the system, suggesting the validity of the LEGI hypothesis.

Crucially, two experiments have revealed quantitative characteristics of the gradient sensing system by using *Dictyostelium* cells that can potentially challenge the LEGI hypothesis. First, by simultaneously visualizing the spatial distribution of PI3K and PIP₃, as well as that of chemoattractant at the single-cell level, Janetopoulos et al have shown that cells in a graded chemoattractant stimulus exhibit localization of the signaling molecules on the membrane in a way that reflects the relative steepness of the

gradient (15). That is, the level of localization of the signaling molecules does not depend on the absolute concentration of chemoattractant but on the difference between the concentration at the front and rear normalized by the concentration at the midpoint. Second, by measuring the adaptive dynamics of activated Ras upon spatially-uniform step increase of chemoattractant at the single-cell level, Takeda et al have demonstrated that the population averages of the response amplitude and response time are determined by the relative increase, or the ratio of the change, of the input stimuli (17, 22). A mathematically idealized response property of this type has been named fold-change detection (FCD), where the entire response shape depends only on the relative change in input signals and not on the absolute change (22–24). To discriminate the two response properties where one refers to relative gradient detection in space and the other in time, we hereafter call the former spatial FCD and the latter temporal FCD. Either the spatial FCD or temporal FCD has been separately reproduced by different models (17, 20, 22). However, it remains elusive what features of the governing equations enable the FCDs. Hence, for example, we do not know if both FCDs are simultaneously achievable. In this paper, we address three questions: (1) Can a model based on the LEGI mechanism account for both FCDs? (2) Does either one of the FCDs automatically implies the other? (3) Does a LEGI model that achieves both FCDs require a specific network topology of the signaling system?

Here, we propose scale-invariance LEGI model, a LEGI-based model that is capable of both spatial and temporal FCDs. Analyses of the model reveal that spatial and temporal FCDs respectively result from two different types of scale invariance, in other words, two symmetries in the model equations. Exploring the systems-level consequences of these two symmetries, we propose spatio-temporal FCD, the ability that allows a system to detect relative changes in spatio-temporal gradients. Finally, these input-output properties are shown to be generic consequences of the symmetries in that they do not depend on the network topology of the system. Our results not only further support the LEGI mechanism by demonstrating its capability for temporal and spatial FCDs, but also suggest scale invariance as an underlying design principle of the directional sensing system.

Models

Scale-invariant LEGI model

Here we describe the scale-invariant LEGI model capable of both temporal and spatial FCDs. The model contains two signaling components, a membrane-bound activator A, which is considered to be the output of the system, and its inhibitor B. Following the standard LEGI framework (11, 18), we here adopt a feedforward regulatory network, where both components A and B are activated by an input signal, i.e., chemoattractant S (Fig. 1). The inhibitor can be detached from the membrane and diffuse inside the cell with fast kinetics; therefore, the inhibitor levels on cell membrane are globally coupled through the cytosolic inhibitor level. Taken together, the dynamics of each component's activity at each point on the cell membrane is described as

$$\begin{aligned}\frac{\partial A}{\partial t} &= k_a \frac{S^n}{S^n + (KB)^n} - k_{-a}A, \\ \frac{\partial B}{\partial t} &= k_b S - k_{-b}B + D(\langle B \rangle - B),\end{aligned}\quad (1)$$

where $k_a, k_{-a}, k_b, k_{-b}, n, K$, and D are constant parameters. $\langle B \rangle$ is the spatially averaged inhibitor level over the membrane, which represents the cytosolic level of inhibitor B. The parameter values are $k_a = 5$, $k_{-a} = 0.5$, $k_b = 0.5$, $k_{-b} = 0.25$, $n = 6$, $K = 1$, and $D = 0.1$. Note that we adopted the high value of the Hill coefficient ($n = 6$) to represent strong amplification of the input signal in the system. We will discuss possible molecular mechanisms for the model equations, especially the one for the nonlinear function, $S^n / (S^n + (KB)^n)$, below and in the Supporting Material.

LEGI models capable of either temporal or spatial FCD but not both

To demonstrate that temporal and spatial FCDs can be implemented independently with each other, here we describe two LEGI-based models as simple examples, which are partially different from the scale-invariant LEGI model. The models contain the same two signaling components as in the scale-invariant LEGI model (Eqs. 1), a membrane-bound activator A and its inhibitor B, and retain the basic network topology of the chemical reaction circuit (Fig. 1). The first of these two models differs from the scale-invariant LEGI model in that inhibitor B on the membrane mediates the binding/unbinding processes of the inhibitor to the membrane:

$$\begin{aligned}\frac{\partial A}{\partial t} &= k_a \frac{S^n}{S^n + (KB)^n} - k_{-a}A, \\ \frac{\partial B}{\partial t} &= k_b S - k_{-b}B + DB(\langle B \rangle - B),\end{aligned}\quad (2)$$

where $k_a, k_{-a}, k_b, k_{-b}, n, K$, and D are constant parameters. The parameter values used for this model are $k_a = 5$, $k_{-a} = 0.5$, $k_b = 0.5$, $k_{-b} = 0.25$, $n = 6$, $K = 1$, $D = 1$.

In the second model, the inhibitor B now directly breaks down the activator A, instead of merely interfering with the synthesis of it:

$$\begin{aligned}\frac{\partial A}{\partial t} &= k_a S - k_{-a}AB, \\ \frac{\partial B}{\partial t} &= k_b S - k_{-b}B + D(\langle B \rangle - B),\end{aligned}\quad (3)$$

where k_a, k_{-a}, k_b, k_{-b} , and D are constant parameters. The parameter values used for this model are $k_a = 0.5$, $k_{-a} = 0.5$, $k_b = 1$, $k_{-b} = 1$, and $D = 2$.

Scale-invariant LEGI model based on a negative feedback loop

Here we describe another scale-invariant LEGI model to show that the feedforward regulatory network is not essential to realize spatial and temporal FCDs. The only difference here is that the interaction between A and B follows what is called a negative feedback loop (Fig., 7a). The equations are

$$\frac{\partial A}{\partial t} = k_a \frac{S^n}{S^n + (KB)^n} - k_{-a}A,$$

$$\frac{\partial B}{\partial t} = k_b AB - k_{-b} B + D(\langle B \rangle - B), \quad (4)$$

where $k_a, k_{-a}, k_b, k_{-b}, n, K$, and D are constant parameters. The parameter values used for this model are $k_a = 0.5, k_{-a} = 0.5, k_b = 2.5, k_{-b} = 0.25, n = 6, K = 1$, and $D = 0.5$,

Numerical method

In numerical computation, we considered circular cell periphery, and discretized the periphery into $N = 100$ points. We utilized MATLAB's "ode45" function for numerical integration of the models.

Results

Responses to spatially-homogeneous time-varying inputs

First we analyze the response of the scale-invariant LEGI model (Eqs. 1; see Models) based on an incoherent feedforward loop (iFFL) (Fig. 1 and Models) to spatially-uniform stimuli. Without gradient stimuli, the model equations become

$$\begin{aligned} \frac{dA}{dt} &= k_a \frac{S^n}{S^n + (KB)^n} - k_{-a} A, \\ \frac{dB}{dt} &= k_b S - k_{-b} B, \end{aligned} \quad (5)$$

because the average inhibitor level B along the cell membrane equals to that at each point, i.e., $\langle B \rangle = B$. Thus, the system is now characterized by three scalar variables A, B and S , which represent the levels of spatially-uniform components. When exposed to step inputs, the activator level A , which is the output signal of the system, shows transient response and adapts to persistent stimuli whereas the inhibitor level B monotonically increases until it reaches a steady-state value (Fig. 2a). The steady-state concentration of each variable is given by

$$A = \frac{k_a}{k_{-a}} \frac{k_{-b}^n}{k_{-b}^n + (Kk_b)^n}, B = \frac{k_b}{k_{-b}} S_0, \quad (6)$$

where S_0 represents the level of the input stimulus at steady state. The steady-state level of the activator A is independent of stimulus level S_0 , meaning that the system shows perfect adaptation. Furthermore, the model responds to the ratio of changes in the input level but not its absolute level, as demonstrated by responses to two successive step inputs with identical fold change (Fig. 2b). Shoval and co-workers have shown that the temporal FCD property results from invariance of the system equations upon a scale transformation of the variables (23). In our model, the temporal FCD property is attributed to the invariance of the equations (Eqs. 5) under the scale transformation

$$(A, B, S) \rightarrow (A, pB, pS) \quad (p > 0), \quad (7).$$

Note that the activator A remains invariant when other variables are multiplied by a scalar p . Intuitively, the invariance means that multiplying an input stimulus S by p does not affect the trajectory of A , whereas the trajectory of B is multiplied by p . Therefore, our model shows the temporal FCD property instead of only perfect adaptation upon spatially-uniform stimuli.

Responses to static spatially-graded inputs

Next we focus on the response of the model to spatially-graded stimuli at steady state. To this end, we simulated the response to linear gradient stimuli in two-dimensional space assuming that the reactions occur on a circular cell membrane. In Figure 3a, the levels of activator A and inhibitor B at points on the membrane are plotted as a function of input level S at the corresponding points. While the inhibitor B is distributed more homogeneously than that of the input stimulus S , the activator A shows a steeper gradient than the input stimulus S ; this means that the gradient signal is amplified. Figure 3b shows the level of activator A and inhibitor B at the front and back of the cell as a function of the absolute input level measured at the center of the cell S_0 with a fixed relative gradient steepness. While the level of inhibitor B increases with the mean stimulus level S_0 , the output A remains constant both at the front and back. Thus, the system's output depends on the relative steepness of the input, i.e., it shows the spatial FCD property. The origin of the spatial FCD property of our model can be understood as follows.

Suppose that the system is in the steady state, i.e., $\frac{\partial A}{\partial t} = \frac{\partial B}{\partial t} = 0$, under a gradient stimulus. Then, the right-hand sides of the model equations (Eqs. 1) are invariant under a scale transformation, $(A, B, S) \rightarrow (A, pB, pS)$. That is, the p -fold change in the input level S can be perfectly compensated by the multiplied pB , and thus the profile of the activator A does not change. Note that here we do not assume that the spatial profile of the input stimulus S is linear. The system shows the spatial FCD property in an arbitrary shape of the gradient of input stimulus.

To illustrate the consequence of the scale invariance, we study the model (Eqs. 1) in one-dimensional geometry where the front and back membrane consisting of single points are connected by cytosol. Here the spatially-graded stimulus is represented by two scalars representing stimulus levels at cell front S_f and at the back S_b with S_f larger than S_b . Thus, the model equations at the front are described as

$$\begin{aligned} \frac{dA_f}{dt} &= k_a \frac{S_f^n}{S_f^n + (KB_f)^n} - k_{-a}A_f, \\ \frac{dB_f}{dt} &= k_b S_f - k_{-b}B_f + D\left(\frac{B_f + B_b}{2} - B_f\right), \end{aligned} \quad (8)$$

and the model equations at the back are given by the same expression by exchanging the subscripts f and b . The analytical steady-state solutions for the concentration of the activator A and the inhibitor B are written as

$$A_f = \left(\frac{k_a}{k_{-a}} \right) \frac{(S_f/\bar{S})^n}{(S_f/\bar{S})^n + K^n (B_f/\bar{S})^n},$$

$$\frac{B_f}{\bar{S}} = \frac{k_b}{k_{-b}} + \frac{k_b}{2(k_{-b} + D)} \frac{(S_f - S_b)}{\bar{S}}, \quad (9)$$

where $\bar{S} = (S_f + S_b)/2$. The steady-state solutions at the back are given by the same expression by exchanging the subscripts f and b . Note that A_f and A_b are dependent only on the relative level of the input stimuli S_f/\bar{S} and S_b/\bar{S} , respectively, i.e., the system shows the spatial FCD property. Therefore, the scale invariance in the model equations results in the normalization of the input stimulus by its spatially-averaged value in its solution.

Responses to complex input stimuli

Several experimental studies have investigated responses to complex input stimuli such as rapid reversal of spatial gradients of chemoattractant (12), stimulation with multiple sources of chemoattractant (15) and a combination of spatially-graded and uniform stimuli (6). To test whether our model can reproduce cell responses to such complex stimuli, we simulated the scale-invariant LEGI model (Eqs. 1) by following the stimulation protocols of those experiments. First, experiments have demonstrated that the gradient of the signaling molecules switches promptly upon reversal of the direction of gradient of chemoattractant (12). The behavior is known to be inconsistent with a model based on the spatial instability in reaction-diffusion system, or ‘‘Turing-type pattern formation’’ (25). Figure 4a shows the level of activator A at the front and the back as a function of time, where the direction of a linear-gradient stimulus is reversed at time $t = 20$. Consistent with the experimental result, our model switches the gradient of the activator A . Second, other experiments have shown that cells, when stimulated with multiple sources of chemoattractant, show localizations of the signaling molecule at multiple sites on the membrane in a way that the degree of localization dynamically follows the strength of the stimulus (15). To confirm the response property of the model, we simulated the response by locating a single point source of stimulus in close proximity to the cell membrane, and then another point source at the opposite site with increasing level of stimulus (Fig. 4b). In consistent with experimental results, the model showed multiple peaks of activator A dynamically following the strength of the input stimuli. Third, another interesting property of the gradient sensing system is its ‘inversed’ responsiveness to a spatially-uniform stimulus: When cells are exposed to a gradient stimulus, then no stimulus (by withdrawing the gradient stimulus), and then a spatially-uniform stimulus, the back of the cell in the gradient stimulus responds more strongly than the front (6). In Figure 4c, at the initial state the cell is exposed to a linear gradient, then the stimulus is withdrawn, and then a uniform stimulation is applied. In agreement with experiment, the cell showed higher response at the back upon exposure to the uniform stimuli. These results would be reproducible by a broad range of LEGI-based models, since they rely on the basic machinery of the system where the range of action of the activator is local and that of the inhibitor is global. The results demonstrate that the scale-invariant LEGI model preserves the properties inherent to a LEGI-based model.

Responses to spatially and temporally graded stimuli

We have shown that our model reproduces both the temporal and spatial FCD properties. However, as is suggested by the analyses so far, the conditions that lead to each property overlap only partially and are not exactly the same (Fig. 5a): For the temporal FCD property, the both equations are invariant upon a scale transformation, excluding the coupling term representing the interaction between different membrane parts, which in our model corresponds to $D(\langle B \rangle - B)$ (Eqs. 1). This is because the coupling term is negligible in the condition due to the spatially uniform environment, i.e., $\langle B \rangle = B$. Let us call this type of invariance temporal FCD symmetry (Fig. 5a). On the other hand, for the spatial FCD property, the equations are invariant including the coupling term but excluding the time derivative terms of the variables. This is because the spatial FCD property refers to a steady-state behavior where $\frac{\partial A}{\partial t} = \frac{\partial B}{\partial t} = 0$. We'll call this type of invariance spatial FCD symmetry (Fig. 5a). Thus, neither the temporal nor spatial FCD property can automatically imply the presence of the other in the LEGI framework.

The discussion above suggests that there exist LEGI-based models that are capable of either temporal or spatial FCD but not both. To demonstrate this, we first consider a model with a partial symmetry (Eqs. 2; see Models). Here, the equations have the coupling term that includes a nonlinear dependence on the difference between the spatial average of inhibitor levels and the inhibitor level at each point. Numerical simulation shows that the model is capable of temporal FCD but not spatial FCD (Fig. 5b and c), consistent with the observation that the system has the temporal FCD symmetry, but lacks the spatial FCD symmetry. Next, we consider another LEGI-based model (Eqs. 3; see Models), where the inhibitor B directly breaks down the activator A instead of interfering with the synthesis of A as in the original model. In contrast to the first model (Eqs. 2), the model shows spatial FCD but not temporal FCD (Fig. 5d and e), which can similarly be understood by the presence of the spatial FCD symmetry, and the absence of the temporal FCD symmetry in the equations describing the system. Note that the ways to break each symmetry in equations are not restricted to the specific functional forms in our exemplification (Eqs. 2 and Eqs. 3).

The independency of spatial and temporal FCDs raises a new question on what is the unique consequence of having both symmetries in one system. We have shown that exposing a system to stimuli changing either in space or time, but not both, can only reveal either of the symmetries, i.e., the spatial or temporal FCD symmetry, in the system. Below, we demonstrate that input stimuli changing in both space and time at the same time allow for the simultaneous presence of both symmetries to manifest themselves in the output of the system. To this end, we simulated the response of our models to two propagating Gaussian waves with the same shape but different absolute levels (Fig. 6a and b). We found that the scale-invariant LEGI model exhibits identical response to two wave stimuli if the two inputs are proportional to each other, $S_1(\mathbf{r}, t) = pS_2(\mathbf{r}, t)$, a property we hereafter call spatio-temporal FCD (Fig. 6c). Specifically, the activator A shows identical spatio-temporal profile in the two input stimuli (Fig. 6c) whereas the inhibitor B depends on the absolute value of the input (Fig. 6d). The invariant response of the activator A is observed irrespective of the speed of the wave (Fig. 6e). In contrast, the models that only have partial symmetry (Eqs. 2 and Eqs. 3) cannot show such behavior, showing deviation from the spatio-temporal FCD property (Fig. 6f and 6g). More precisely, the model with only the temporal FCD symmetry shows significant dependence on the absolute level of the input stimulus S when the wave speed is low (Fig. 6f, top panels), whereas the model with only the spatial FCD symmetry shows similar non-scaling behavior when the wave speed is high (Fig. 6f, bottom panels). These phenomena can be understood by realizing that, if the speed of a traveling wave is fast enough, the traveling wave becomes essentially spatially-

uniform impulse-like stimulus to the cells. Hence, a model with the temporal FCD symmetry shows approximately rescaling response property to such a stimulus, although a model that lacks the symmetry does not. Similarly, if the speed of a traveling wave is sufficiently slow, the traveling wave becomes more similar to a static spatially-graded stimulus. Under such a stimulus, the spatial FCD symmetry achieves rescaling response approximately, while the temporal FCD symmetry does not. Therefore, these results demonstrate that the rescaling responses to wave stimuli manifest the simultaneous presence of the two symmetries in the system.

Behavior of a scale-invariant model with a different network topology

The interaction between signaling components in the scale-invariant LEGI model (Eqs. 1) follows an iFFL network topology (Fig 1), where the stimulus S activates both the activator A and the inhibitor B (Fig. 1). Although we have discussed the functional importance of the symmetry of the system so far, it has remained unanswered whether the symmetries require the specific network topologies or not. We found that, within the LEGI framework where the activator operates locally and the inhibitor globally, it is also possible to implement the system based on a negative feedback interaction (Fig. 6a) with exactly the same symmetry as the rescaling LEGI model (Eqs. 4; see Models). This model also shows temporal FCD (Fig. 6b), spatial FCD (Fig. 6c) and spatio-temporal FCD (Fig. 6d) as would be expected from the presence of both symmetries. Although the detailed feature of the response, such as the overshoot response in the negative feedback model (Fig. 6b), can be specific to a type of network topology, the results clearly demonstrates that the relation between the symmetries in the equations and the response properties is generic without depending on the specific network topology of the system.

Discussion

Quantitative characterizations of input-output relations of a biological system place constraints on the possible mechanisms that may underlie the system, by providing criteria that a model of the system must satisfy. In this study, inspired by quantitative experiments on the eukaryotic directional sensing system that have revealed the temporal and spatial FCD properties (15, 17), we explored mathematical conditions that endows a model of the signaling system with both FCD properties. We have identified the two symmetry conditions in governing equations responsible for the respective FCD properties (Fig. 5a). Given the symmetries, both of the temporal and spatial FCD properties do not require fine-tuning of the parameter values of the system. Furthermore, we have demonstrated that the model can reproduce responses to more complex stimuli such as ones from multiple sources (Fig. 4). In addition, although a study on *Dictyostelium* has supported feedforward mechanism (17), we have demonstrated that the rescaling behaviors are achievable independent of the network topology (Fig. 7). The results support the validity of the LEGI framework as a core mechanism of the directional sensing system.

Because the LEGI framework does not specify the details of mathematical models, many versions of LEGI-based models have been proposed with various assumptions. We note that several models reported so far are capable of either temporal or spatial FCD (see Supporting Material). Regarding temporal FCD, Adler et al (22) have explained rescaled responses in time revealed by Takeda et al (17) by

using a model with the temporal FCD symmetry. However, this model assumes spatial uniformity of the stimulus and therefore does not explain the spatial gradient sensing of the system. On the other hand, as pointed out by Nakajima et al (14), several models are known to have the spatial FCD property. For example, Levchenko and Iglesias, in their pioneering work (18), have proposed LEGI-based models that are capable of the spatial FCD property. These models satisfy the spatial FCD symmetry but not the temporal FCD symmetry without adding further assumption (see Supporting Material). Note that lack of the symmetries does not necessarily mean that the model is inappropriate or inferior to those with the symmetries. For example, a detailed experimental study have revealed that the activity of Ras upon spatially-uniform stimulation shows slightly imperfect adaptation in *Dictyostelium* (14); this means that the temporal FCD property, which entails perfect adaptation (23, 24), is only approximately realized. Still, we believe that elucidating the relation between the symmetries and the rescaled responses is helpful to understand and modify mathematical models of the gradient sensing system. For further analyses on variants of LEGI-based models, see the Supporting Material.

From the experimental perspective, most studies on the directional sensing system so far, except a few most recent studies described below, have investigated responses to either temporal or spatial gradient but not both. Although such experiments have successfully revealed the temporal and spatial FCD properties, our results suggest that using spatio-temporal stimuli such as traveling wave can provides further insights into the system: responses to such stimuli can manifest the simultaneous presence of the two symmetries in the system. Importantly, given the ubiquity of cellular responses where input stimuli with different dynamic properties activate different subsystems in the signal transduction (26, 27), the question remains whether the temporal and spatial FCDs result from the same single machinery or different signaling subsystems in the gradient sensing.

Recent advances in microfluidic technology have made it possible to generate traveling wave stimuli of chemoattractant in a flow chamber (14, 28). Although the rescaling behavior in wave stimuli remain unaddressed experimentally, such experiments have revealed that the directional sensing system of *Dictyostelium* exhibits highly asymmetric responses at the front and back of the waves; the activated form of Ras, an output signal of the gradient sensing system, shows strong localization toward the side of higher chemoattractant concentration only in the wavefront, where the chemoattractant concentration is increasing. This explains the unidirectional migration of the cells towards incoming waves (14, 28). The asymmetric behavior has been successfully reproduced with LEGI-based models (14, 28). As argued in the study (14), higher amplification of input signal is crucial for the behavior. By adopting comparatively high amplification parameter (e.g., n in Eqs. 1), the scale-invariant LEGI model also exhibits highly asymmetric responses at the wavefront and waveback (Fig. 6c). Therefore, the rescaling behavior and the asymmetric response are compatible with each other.

What is the function of spatio-temporal FCD in eukaryotic chemotaxis? A similar question has been asked about temporal FCD in the context of prokaryotic chemotaxis (23, 29). When a prokaryotic cell moves around in an input (i.e., chemoattractant) field, the cell only senses the local input level, i.e., no gradient information along the cell body is exploited. Instead, previous studies indicate that spatial gradient of the input is estimated from temporal changes of the input level in incessant motion of the cells (30). In this setup, it has been shown that the temporal FCD property ensures that the cell's search depends only on the shape of the input field, where the shapes of two input fields are the same if one matches the other by a constant multiple (23). In other words, the search is independent of the absolute

level of the input field. Such an input field with scalar symmetry is considered to be commonplace in natural environments because the solutions for the advection-diffusion equation are often linear in the magnitude of source strength (23). In eukaryotic chemotaxis, the situation is more complicated because the cells sense temporal and spatial gradient in an input field (14, 28). Therefore, neither temporal nor spatial FCD alone can ensure that the cell's search is independent of the absolute level of the input field. By contrast, spatio-temporal FCD ensures invariant search irrespective of its absolute level. In that sense, spatio-temporal FCD in eukaryotic chemotaxis can be considered as a functional equivalent of temporal FCD in prokaryotic chemotaxis.

For the sake of simplicity, we have implemented the model without resorting to the known details of the molecular network of the directional sensing system. The phenomenological approach allowed us to clearly analyze the relation between the symmetries and their behavioral consequences, i.e., temporal FCD, spatial FCD and spatio-temporal FCD. However, a more detailed model is still helpful to capture the still-unknown exact molecular mechanism of the system. For example, we adopted nonlinear function $S^n/(S^n + (KB)^n)$ in Eqs. 1 without specifying the underlying mechanism. Such a sigmoidal nonlinearity is known to emerge based on various mechanisms such as cooperative interactions of signaling molecules (31), zero-order ultrasensitivity (32), and multistep effects (33), just to name a few. On the other hand, in the nonlinear function, the variable B works as a memory in the sense that B alters A 's sensitivity depending on the recent history of S . A similar input function can be seen in the model for bacterial chemotaxis too where the molecular mechanism for the memory has been identified as the methylation level of the chemoattractant receptors (34–36). We discuss a biochemical network that enables such a sensitivity control in the Supporting Material.

In summary, we have combined two major concepts in quantitative biology, namely, FCD and the LEGI framework, and have proposed a new system-level mechanism to explain the rescaling behaviors of the gradient sensing system. We hope that our results promote understandings of the detection of spatio-temporal chemical gradients in eukaryotic chemotaxis.

Figure captions

Fig. 1. Schematic representation of the scale-invariant LEGI model. The model describes the dynamics of the levels of activator A and inhibitor B upon chemoattractant stimulus S . The arrows and the bar-ended arrow represent excitatory and inhibitory regulations between the signaling components, respectively.

Fig. 2. Temporal fold-change detection (FCD) of the scale-invariant LEGI model in response to spatially uniform stimuli. The insets show the input variable S (green). (a) Trajectories of the activator level A (red) and the inhibitor level B (blue) upon single step input. (b) A trajectory of the activator level A upon two-step inputs with the identical fold change ($p = 5$) but different absolute levels.

Fig. 3. Spatial FCD of the scale-invariant LEGI model upon static gradient stimuli. The input profile follows $S(x,y) = S_0 + \Delta S x$, where the origin of the spatial coordinate x is located at the cell center. (a) Amplified response in the activator level A . The activator level A (red circle) and inhibitor level B (blue circle) are plotted against the input level S at each point on the cell periphery with both A and B

normalized by the value at the center of the cell. The input stimulus used is $S_0 = 0.1$ and $\Delta S = 0.01$. The black line indicates normalized S , which represents unamplified response. (b) The activator level A (red) and inhibitor level B (blue) at the cell front (solid line) and back (broken line) are plotted as a function of the mid-point input level S_0 . The relative gradient is fixed as $\Delta S = 0.1 S_0$.

Fig. 4. Responses of the scale-invariant LEGI model to complex stimuli. (a) The trajectories of the activator A at the cell front (solid line) and back (dotted line) are plotted upon sudden reversal of a linear gradient ($S(x, y) = S_0 + \Delta S x$, $S_0 = 1$ and $\Delta S = \pm 0.1$) at $t = 20$. The inset shows spatial profile of the activator level A at $t = 0$. (b) Responses to two point sources of input stimuli where the input profile is defined as $S(x, y) = C_1 \exp[-((x + x_0)^2 + y^2)/2V] + C_2 \exp[-((x - x_0)^2 + y^2)/2V]$ ($x_0 = 7.5$ and $V = 4$). The positions of the point sources are indicated by the purple squares. (Top left) Spatial profile of the activator level A at steady state in one point source stimulus, i.e., $C_1 = 1$ and $C_2 = 0$. (Bottom left) Spatial profile of the activator level A at steady state in two point source stimuli, i.e., $C_1 = C_2 = 1$. (Right) Time series of the activator A at the cell front (solid line) and back (dashed line) upon application of another point source of S at $t = 0$ at the other side of the cell. The strength of the second signal C_2 is dynamically controlled as shown in the inset. (c) Responses of the model upon sequential change of the input spatio-temporal profile, where spatially graded stimulus ($S(x, y) = S_0 + \Delta S x$, $S_0 = 1$ and $\Delta S = 0.15$) (top left), then no stimulus (top middle) and then a spatially-homogeneous stimulus ($S_0 = 0.3$) (top right) are applied. Spatial profiles of the activator A at corresponding time points are shown at the bottom.

Fig. 5. Two types of symmetry in the scale-invariant LEGI model. (a) Temporal FCD symmetry refers to the scale invariance of the equations excluding the coupling term. Spatial FCD symmetry means the scale invariance of the equations excluding the time derivative terms. (b) A trajectory of the activator level A of the model that only has the spatial FCD symmetry (Eqs. 2; see Models) upon two-step inputs with the identical fold change ($p = 5$) but different absolute levels. The inset shows the input variable S . (c) The activator level A (red) and inhibitor level B (blue) at the cell front (solid line) and back (broken line) are plotted as a function of the mid-point input level S_0 for the model that only has the temporal FCD symmetry. The relative gradient is fixed as $\Delta S = 0.1 S_0$. (d, e) For the model that only has the spatial FCD symmetry (Eqs. 3; see Models), the responses are plotted as in (b, c).

Fig. 6. Spatio-temporal FCD under wave stimuli. The spatio-temporal profile of the traveling wave stimuli is defined by the Gaussian shape as $S(x, y, t) = s_0 \exp[(x - x_0 - w t)^2/2V] + s_b$. Below, $S_{\text{slow}}(x, y, t)$ is defined with the wave velocity $w = 0.5$, while $S_{\text{fast}}(x, y, t)$ is defined with $w = 5$. The width of the wave V , the initial position x_0 , and the basal stimulus level s_b are fixed at $V = 100$, $x_0 = 50$, and $s_b = 0.1$, respectively, in both wave stimuli. We use $p = 10$ for the fold-change parameter. (a) Schematic representation of the numerical experiment where a wave stimulus is applied to a cell. (b) The input level S at the cell front (solid line) and back (broken line) under $S_{\text{slow}}(x, y, t)$. (c) Trajectories of the activator level A at the cell front (solid line) and back (broken line) under S_{slow} (red) and pS_{slow} (blue) are plotted for the scale-invariant model (Eqs. 1; see Models). (d) Trajectories of the inhibitor level B are plotted as in (c). (e) For the scale-invariant LEGI model (Eqs. 1), spatio-temporal profiles of the activator level A along the cell periphery are plotted under wave stimuli S_{slow} (top left), pS_{slow} (top right), S_{fast} (bottom left), and pS_{fast} (bottom right), respectively. Note that each point at the cell periphery is indicated by an angle expressed in radians from 0 (cell front) to π (cell back). (f) Responses of the model that only has the temporal FCD symmetry (Eqs. 2; see Models) are plotted as in (e). (g) Responses of the model that only has the spatial FCD symmetry (Eqs. 3; see Models) are plotted as in (e).

Fig. 7. Responses of the scale-invariant LEGI model with a feedback network topology. (a)

Schematic representation of the regulatory network of the model (Eqs. 4; see Models). (b) A trajectory of the activator level A upon two-step inputs with the identical fold change ($p = 5$) but different absolute levels. The inset shows the input variable S . (c) The activator A (red) and inhibitor B (blue) at the cell front (solid line) and back (broken line) under linear profiles of gradient, $S(x,y) = S_0 + \Delta S x$, are plotted as a function of the mid-point input level S_0 . The relative gradient is fixed as $\Delta S = 0.1 S_0$. (d) Responses to wave stimuli are visualized as in Figures 6e. Specifically, spatio-temporal profiles of the activator level A along the cell periphery under wave stimuli S_{slow} (top left), pS_{slow} (top right), S_{fast} (bottom left) and pS_{fast} (bottom right), respectively.

Author Contributions

K.K. and Y.K. designed research, performed research, analyzed data and wrote the paper. K.K. and Y.K. contributed equally to this work.

Acknowledgments

We thank S. Sawai and the members of the Sawai lab for discussions, M. Hamidi, and T. S. Shimizu for comments on the manuscript. This work is supported by The Paul G. Allen Family Foundation and the Foundation for Fundamental Research on Matter (FOM), which is part of the Netherlands Organisation for Scientific Research (NWO) (to K. K.) and the Platform Project for Supporting in Drug Discovery and Life Science Research (Platform for Dynamic Approaches to Living Systems) from Japan Agency for Medical Research and Development (AMED) (to Y. K.).

References

1. Iglesias, P.A., and P.N. Devreotes. 2008. Navigating through models of chemotaxis. *Curr. Opin. Cell Biol.* 20: 35–40.
2. Dormann, D., and C.J. Weijer. 2003. Chemotactic cell movement during development. *Curr. Opin. Genet. Dev.* 13: 358–364.
3. Swaney, K.F., C.-H. Huang, and P.N. Devreotes. 2010. Eukaryotic chemotaxis: a network of signaling pathways controls motility, directional sensing, and polarity. *Annu. Rev. Biophys.* 39: 265–289.
4. Schneider, I.C., and J.M. Haugh. 2006. Mechanisms of gradient sensing and chemotaxis: Conserved pathways, diverse regulation. *Cell Cycle.* 5: 1130–1134.

5. Xiao, Z., N. Zhang, D.B. Murphy, and P.N. Devreotes. 1997. Dynamic distribution of chemoattractant receptors in living cells during chemotaxis and persistent stimulation. *J. Cell Biol.* 139: 365–74.
6. Xu, X., M. Meier-Schellersheim, J. Yan, and T. Jin. 2007. Locally controlled inhibitory mechanisms are involved in eukaryotic GPCR-mediated chemosensing. *J. Cell Biol.* 178: 141–153.
7. Janetopoulos, C., T. Jin, and P. Devreotes. 2001. Receptor-Mediated Activation of Heterotrimeric G-Proteins in Living Cells. *Science* (80-.). 291: 2408–2411.
8. Wu, L., R. Valkema, P.J.M. Van Haastert, and P.N. Devreotes. 1995. The G protein beta subunit is essential for multiple responses to chemoattractants in *Dictyostelium*. *J. Cell Biol.* 129: 1667–1675.
9. Weeks, G., and G.B. Spiegelman. 2003. Roles played by Ras subfamily proteins in the cell and developmental biology of microorganisms. *Cell. Signal.* 15: 901–909.
10. Iglesias, P.A. 2009. Spatial regulation of PI3K signaling during chemotaxis. *Wiley Interdiscip. Rev. Syst. Biol. Med.* 1: 247–253.
11. Parent, C.A., and P.N. Devreotes. 1999. A Cell 's Sense of Direction. *Science* (80-.). 284: 765–770.
12. Parent, C.A., B.J. Blacklock, W.M. Froehlich, D.B. Murphy, and P.N. Devreotes. 1998. G protein signaling events are activated at the leading edge of chemotactic cells. *Cell.* 95: 81–91.
13. Sasaki, A.T., C. Chun, K. Takeda, and R.A. Firtel. 2004. Localized Ras signaling at the leading edge regulates PI3K, cell polarity, and directional cell movement. *J. Cell Biol.* 167: 505–518.
14. Nakajima, A., S. Ishihara, D. Imoto, and S. Sawai. 2014. Rectified directional sensing in long-range cell migration. *Nat. Commun.* 5: 1–14.
15. Janetopoulos, C., L. Ma, P.N. Devreotes, and P.A. Iglesias. 2004. Chemoattractant-induced phosphatidylinositol 3,4,5-trisphosphate accumulation is spatially amplified and adapts, independent of the actin cytoskeleton. *Proc. Natl. Acad. Sci. U. S. A.* 101: 8951–8956.
16. Xu, X. 2004. Quantitative Imaging of Single Live Cells Reveals Spatiotemporal Dynamics of Multistep Signaling Events of Chemoattractant Gradient Sensing in *Dictyostelium*. *Mol. Biol. Cell.* 16: 676–688.
17. Takeda, K., D. Shao, M. Adler, P.G. Charest, W.F. Loomis, H. Levine, A. Groisman, W.-J. Rappel, and R. a Firtel. 2012. Incoherent feedforward control governs adaptation of activated ras in a eukaryotic chemotaxis pathway. *Sci. Signal.* 5: ra2.
18. Levchenko, A., and P.A. Iglesias. 2002. Models of eukaryotic gradient sensing: application to chemotaxis of amoebae and neutrophils. *Biophys. J.* 82: 50–63.
19. Levine, H., D.A. Kessler, and W.-J. Rappel. 2006. Directional sensing in eukaryotic chemotaxis: a balanced inactivation model. *Proc. Natl. Acad. Sci. U. S. A.* 103: 9761–9766.
20. Ma, L., C. Janetopoulos, L. Yang, P.N. Devreotes, and P.A. Iglesias. 2004. Two complementary, local excitation, global inhibition mechanisms acting in parallel can explain the chemoattractant-induced regulation of PI(3,4,5)P3 response in *dictyostelium* cells. *Biophys. J.* 87: 3764–3774.

21. Wang, C.J., A. Bergmann, B. Lin, K. Kim, and A. Levchenko. 2012. Diverse sensitivity thresholds in dynamic signaling responses by social amoebae. *Sci. Signal.* 5: ra17.
22. Adler, M., A. Mayo, and U. Alon. 2014. Logarithmic and Power Law Input-Output Relations in Sensory Systems with Fold-Change Detection. *PLoS Comput. Biol.* 10: e1003781.
23. Shoval, O., L. Goentoro, Y. Hart, A. Mayo, E. Sontag, and U. Alon. 2010. Fold-change detection and scalar symmetry of sensory input fields. *Proc. Natl. Acad. Sci. U. S. A.* 107: 15995–16000.
24. Goentoro, L., O. Shoval, M.W. Kirschner, and U. Alon. 2009. The Incoherent Feedforward Loop Can Provide Fold-Change Detection in Gene Regulation. *Mol. Cell.* 36: 894–899.
25. Jilkine, A., and L. Edelstein-Keshet. 2011. A comparison of mathematical models for polarization of single eukaryotic cells in response to guided cues. *PLoS Comput. Biol.* 7.
26. Purvis, J.E., and G. Lahav. 2013. Encoding and Decoding Cellular Information through Signaling Dynamics. *Cell.* 152: 945–956.
27. Yosef, N., and A. Regev. 2011. Impulse control: Temporal dynamics in gene transcription. *Cell.* 144: 886–896.
28. Skoge, M., H. Yue, M. Erickstad, A. Bae, H. Levine, A. Groisman, W.F. Loomis, and W.-J. Rappel. 2014. Cellular memory in eukaryotic chemotaxis. *Proc. Natl. Acad. Sci.* 111: 14448–14453.
29. Lazova, M.D., T. Ahmed, D. Bellomo, R. Stocker, and T.S. Shimizu. 2011. Response rescaling in bacterial chemotaxis. .
30. Segall, J.E., S.M. Block, and H.C. Berg. 1986. Temporal comparisons in bacterial chemotaxis. *Proc. Natl. Acad. Sci. U. S. A.* 83: 8987–91.
31. Sourjik, V. 2004. Receptor clustering and signal processing in *E. coli* chemotaxis. *Trends Microbiol.* 12: 569–76.
32. Goldbeter, A., and D.E. Koshland. 1981. An amplified sensitivity arising from covalent modification in biological systems. *Proc. Natl. Acad. Sci. U. S. A.* 78: 6840–6844.
33. Goldbeter, A., and D.E. Koshland. 1984. Ultrasensitivity in biochemical systems controlled by covalent modification. Interplay between zero-order and multistep effects. *J. Biol. Chem.* 259: 14441–14447.
34. Shimizu, T.S., Y. Tu, and H.C. Berg. 2010. A modular gradient-sensing network for chemotaxis in *Escherichia coli* revealed by responses to time-varying stimuli. *Mol. Syst. Biol.* 6.
35. Tu, Y. 2013. Quantitative modeling of bacterial chemotaxis: signal amplification and accurate adaptation. *Annu. Rev. Biophys.* 42: 337–59.
36. Tu, Y., T.S. Shimizu, and H.C. Berg. 2008. Modeling the chemotactic response of *Escherichia coli* to time-varying stimuli. *Proc. Natl. Acad. Sci. U. S. A.* 105: 14855–60.

Fig. 1

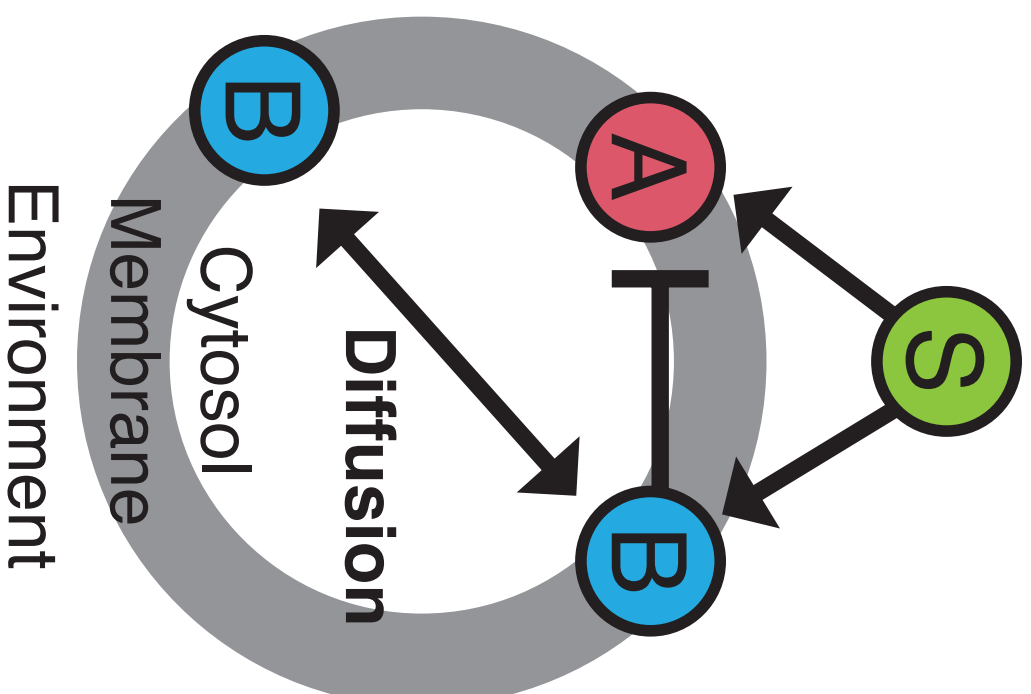
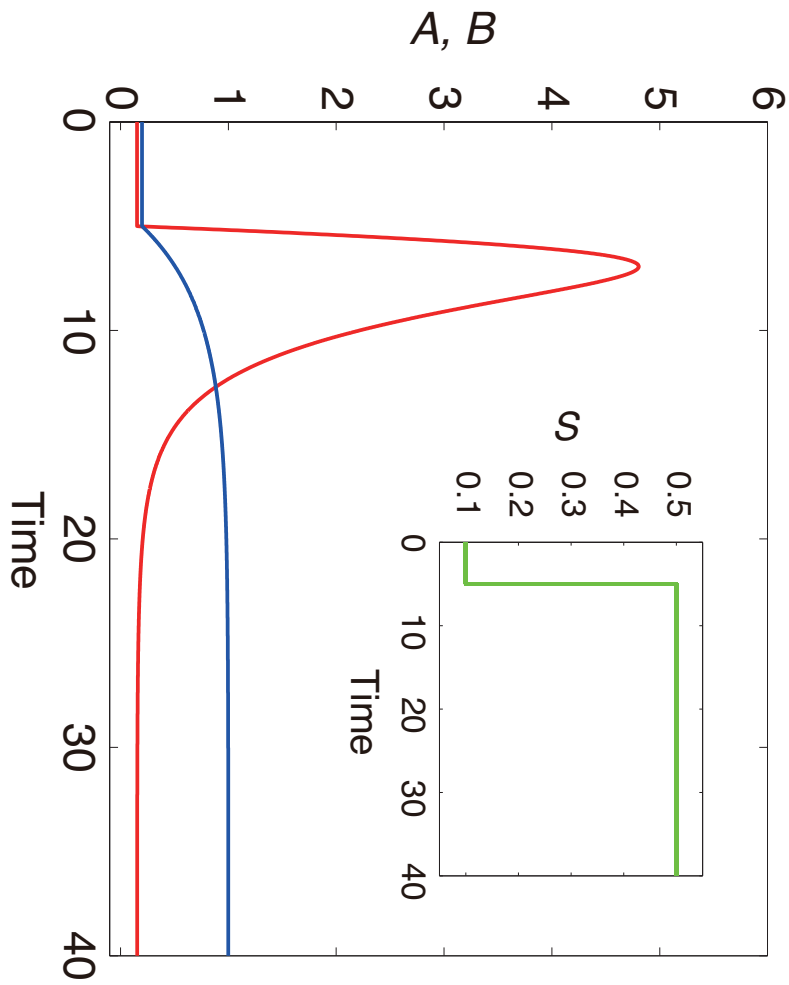


Fig. 2

a



b

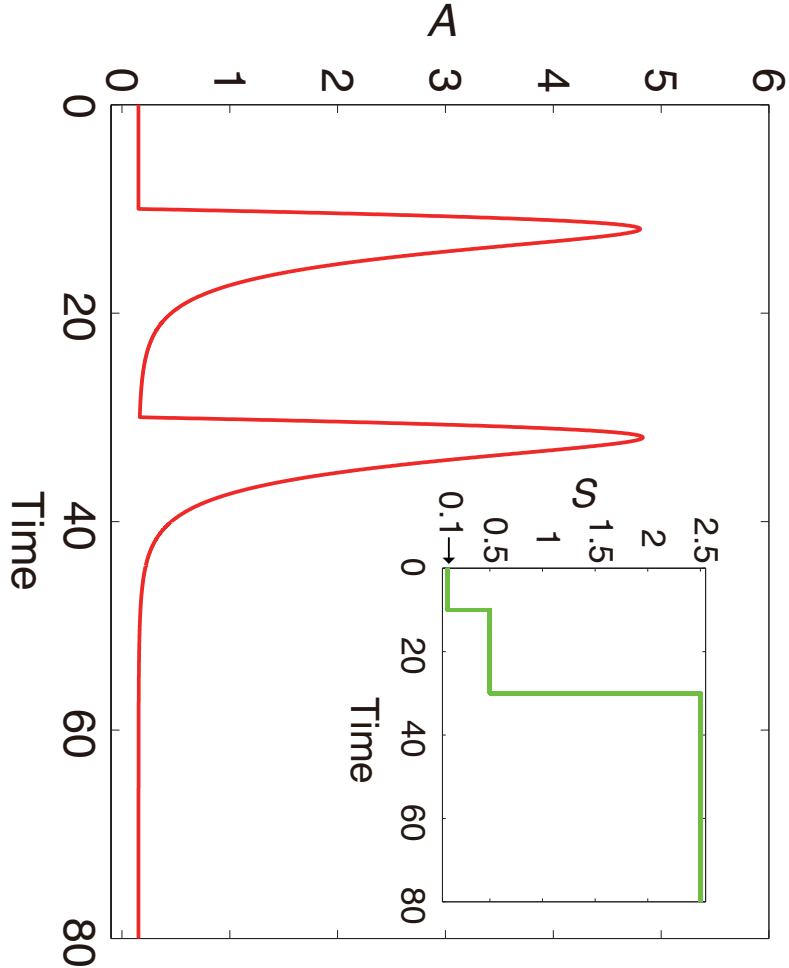
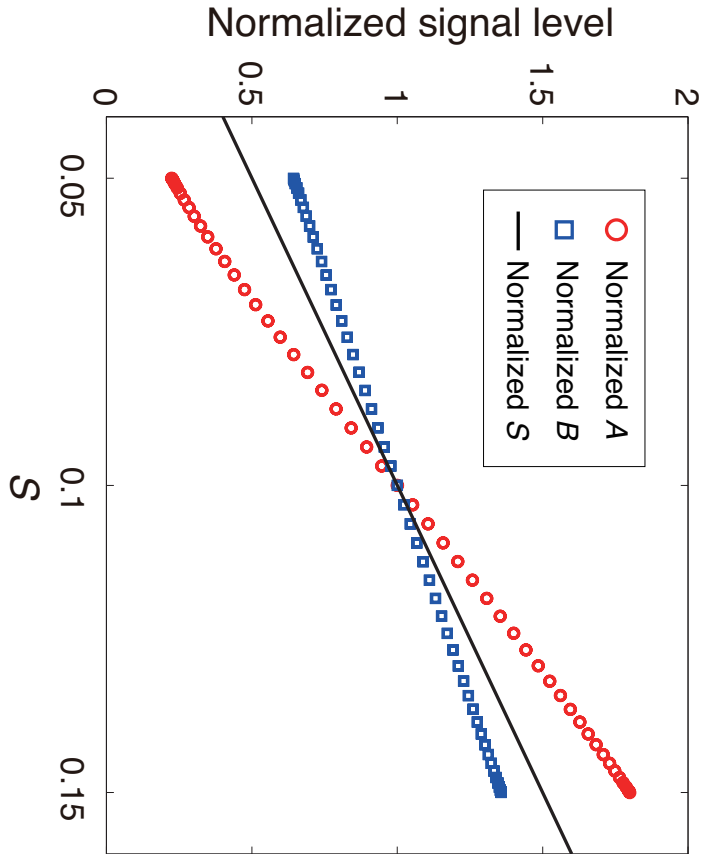


Fig. 3

a



b

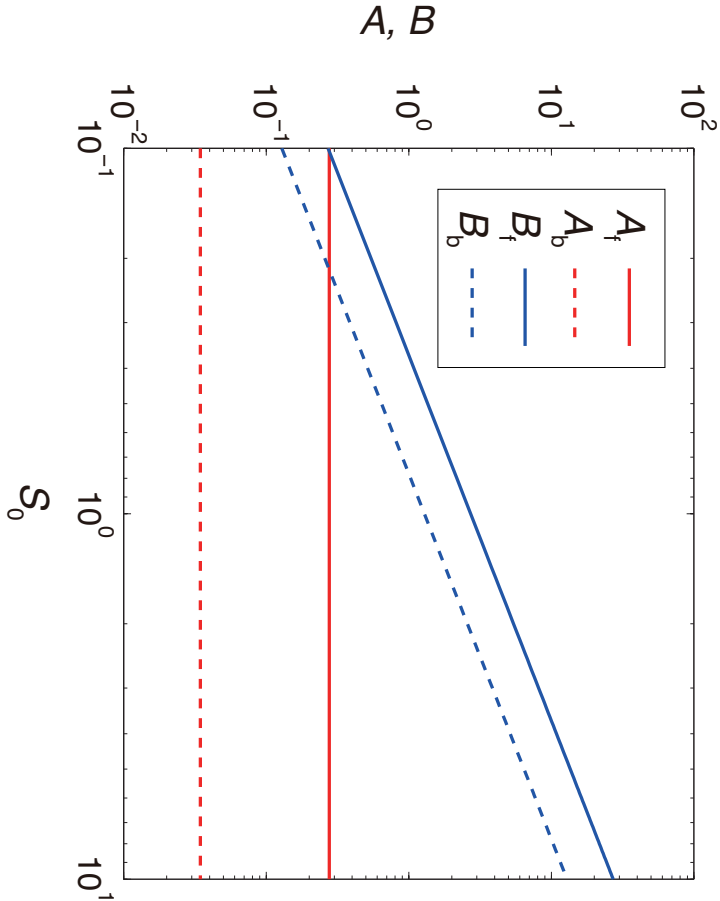
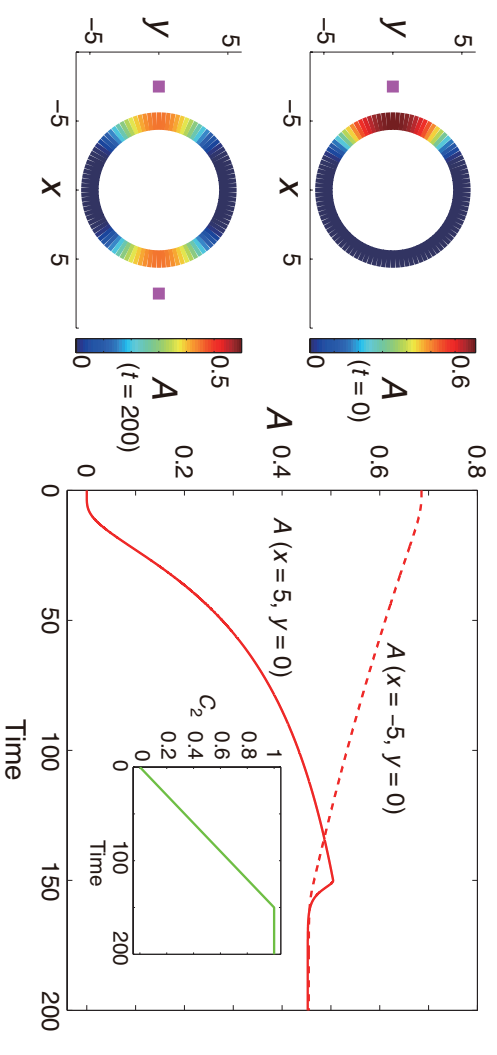
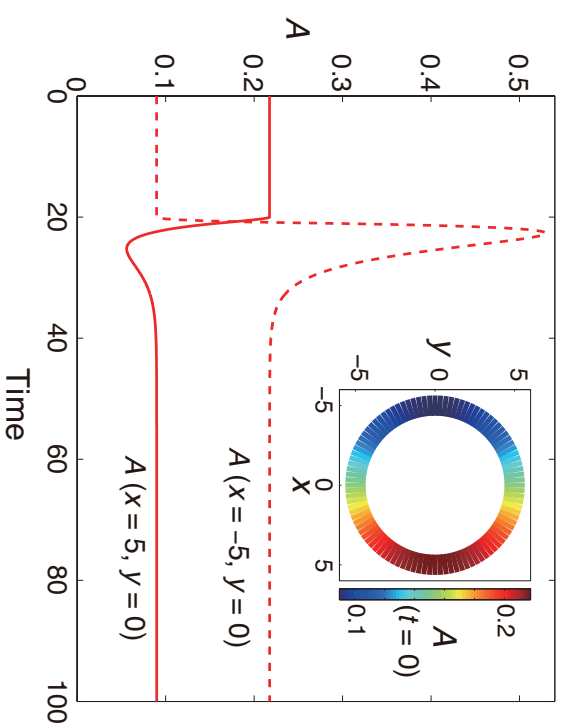


Fig. 4

b



c

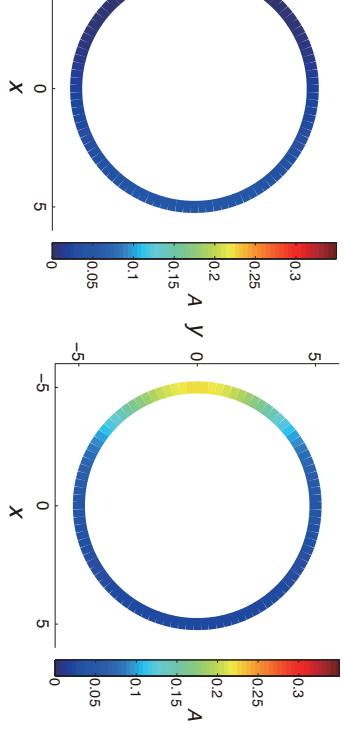
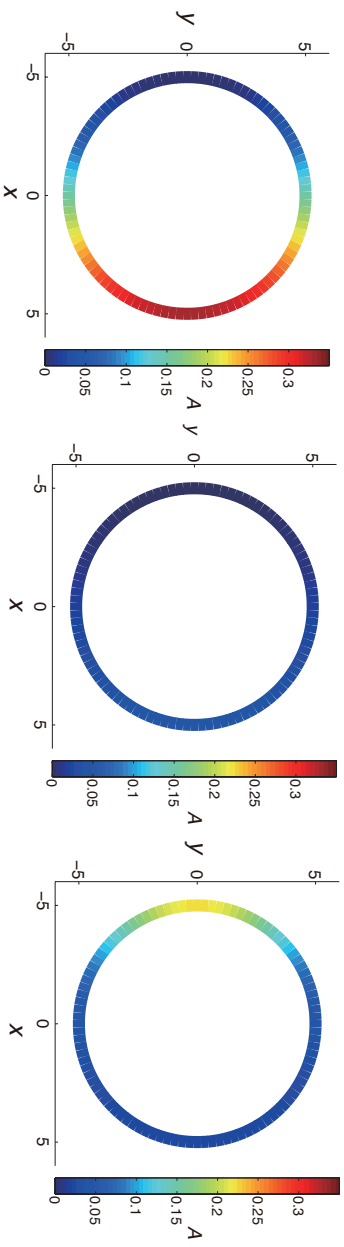
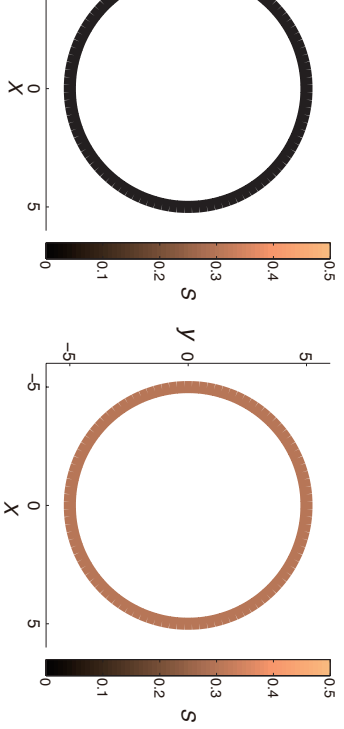
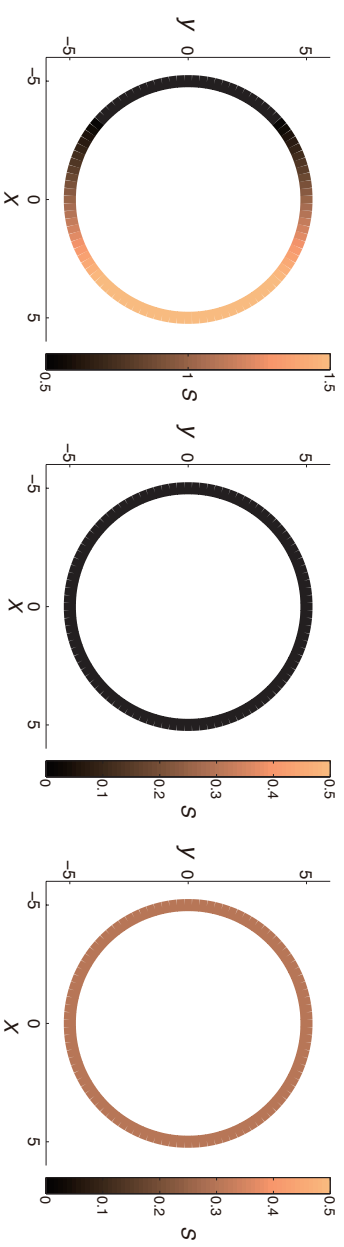
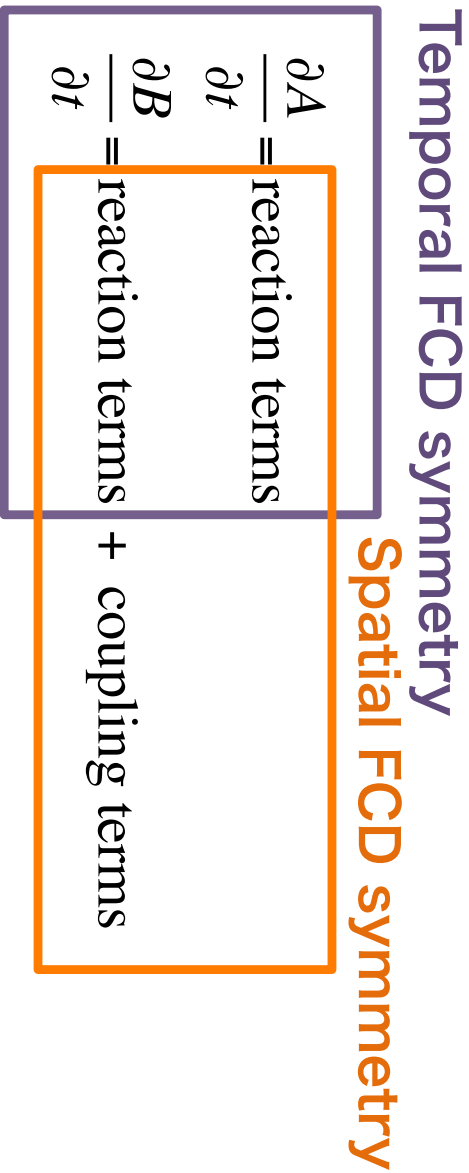
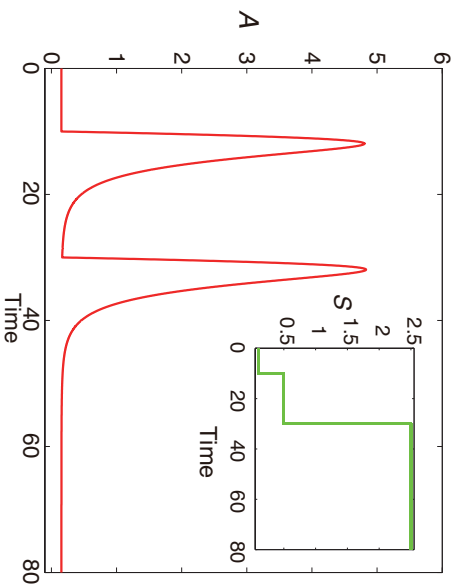


Fig. 5

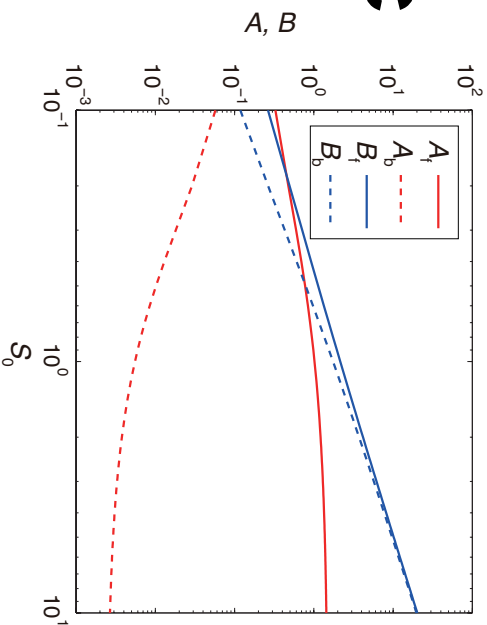
a



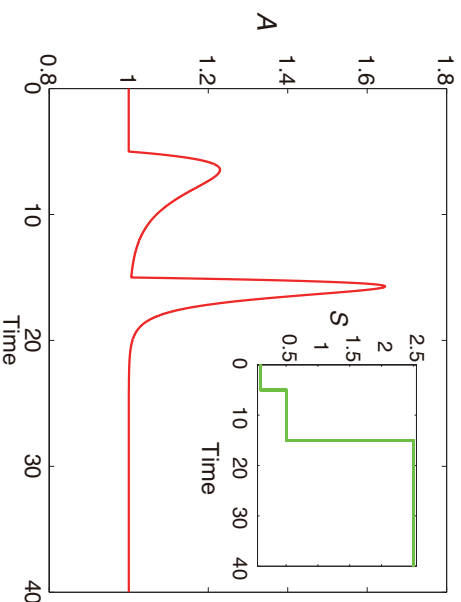
b



c



d



e

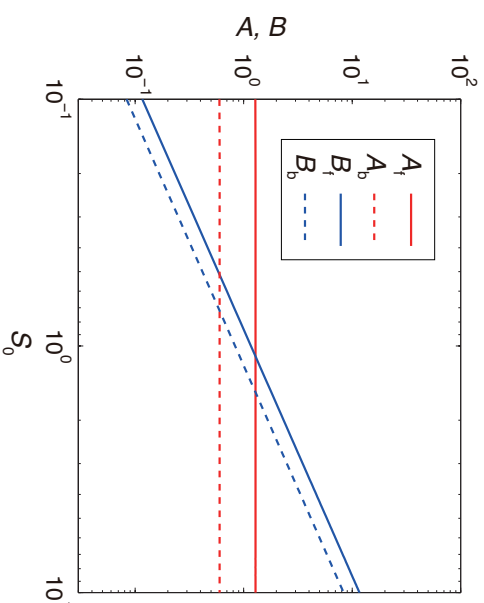


Fig. 6

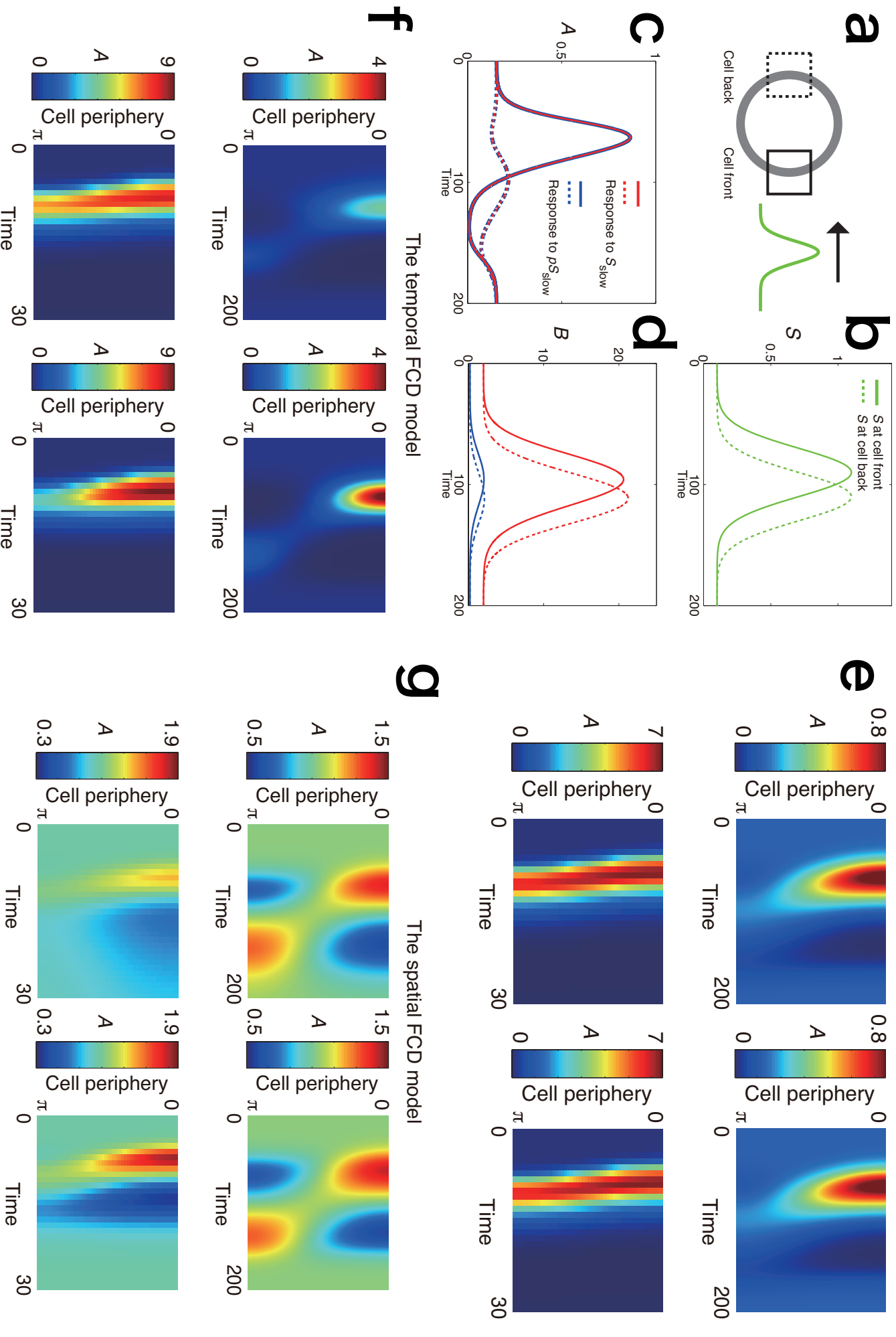
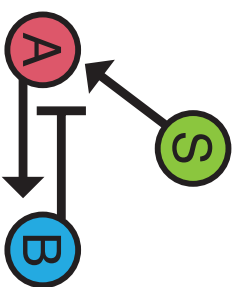
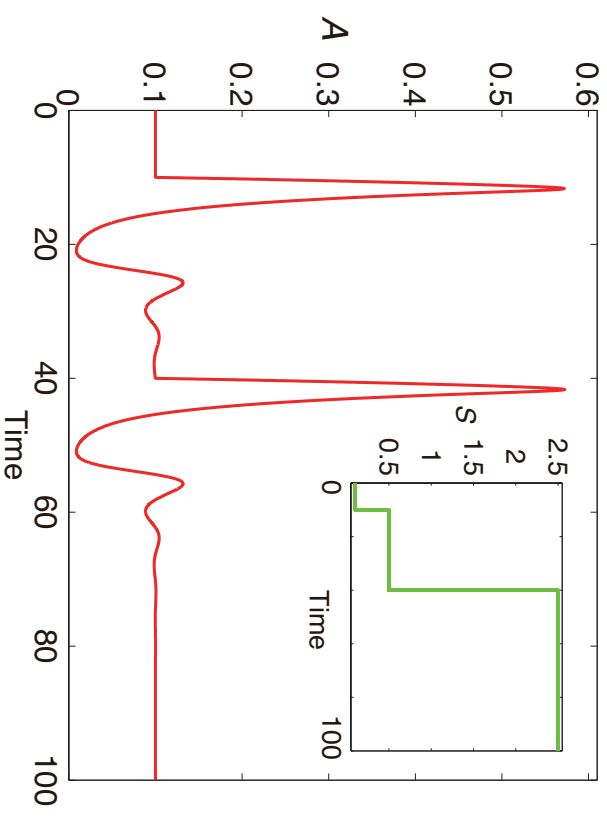


Fig. 7

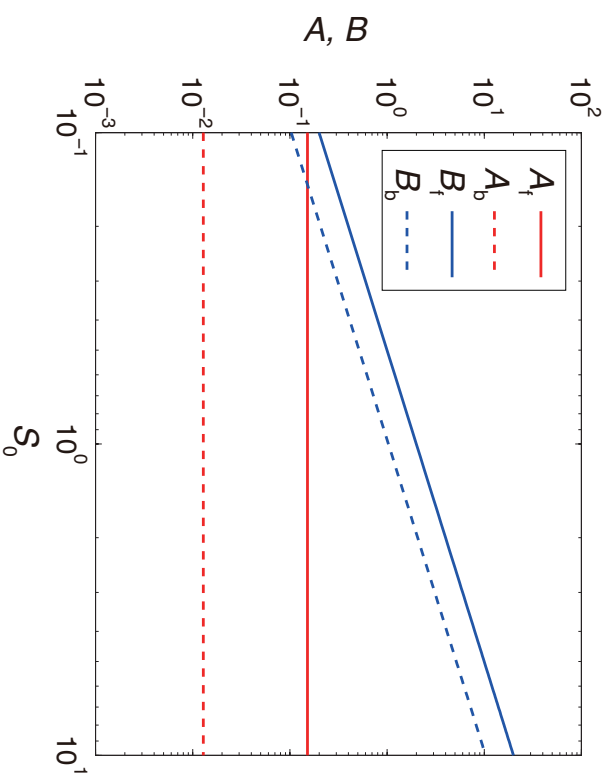
a



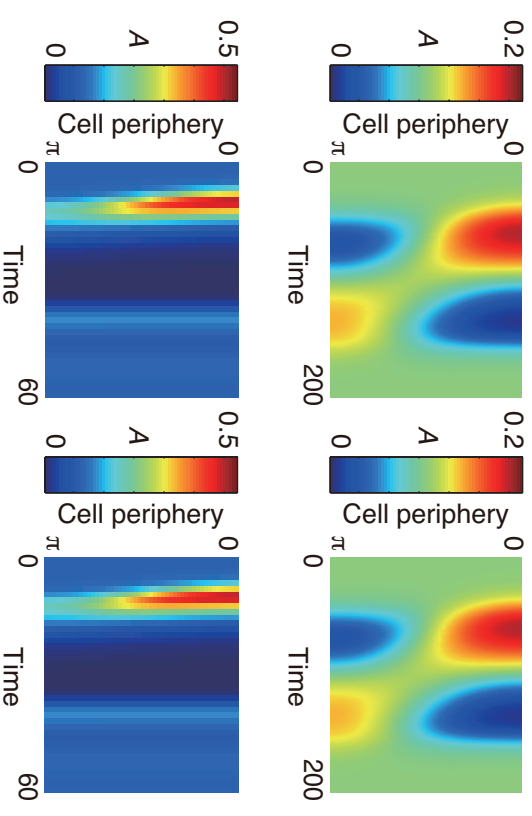
b



c



d



Supporting Material

Earlier models for the eukaryotic gradient sensing system and their symmetric properties

In the main text, we have shown that, based on the LEGI-framework (1), the spatial and temporal FCDs can be achieved respectively by two different scale-invariant properties in a governing equation, i.e., the temporal and spatial FCD symmetry. The two symmetries can be implemented in a mathematical model independently of each other (Fig. 5). The scale-invariant LEGI model (Eqs. 1) satisfies the two symmetries at the same time, and thus the model shows characteristic rescaled responses to stimuli that change in both space and time like traveling wave stimuli (Fig. 6). Among the two symmetric properties, the temporal FCD symmetry and the system-level consequence, i.e., temporal FCD, have been investigated extensively based on ordinary differential equation systems (2, 3) including the model of the directional sensing system in spatially-homogeneous stimuli (4). Concerning the spatial FCD, although several LEGI-based models have the spatial FCD property as pointed out by Nakajima et al (5), the symmetric property of the governing equations of the models, to our best knowledge, have not been studied explicitly. Below, we analyze representative earlier models with spatial dimension in terms of their symmetric properties.

(i) Levchenko-Iglesias models (6)

In the pioneering work by Levchenko and Iglesias (6), LEGI-based models of biochemical circuits have been proposed to describe the response properties of the gradient sensing system. They have assumed that the signaling component characterizing the response is found in both an active, R^* , and an inactive, R , states. The conversion from R^* to R is mediated by the inactivator I and the opposite reaction is mediated by the activator A . Both of the activator A and inactivator I are activated by chemoattractant S . The first model equations they have proposed (Fig. 3A in (6)) are

$$\begin{aligned}\frac{\partial A}{\partial t} &= -k_{-A}A + k_AS, \\ \frac{\partial I}{\partial t} &= -k_{-I}I + k'_IS + D\nabla^2 I, \\ \frac{\partial R^*}{\partial t} &= -k_{-2}IR^* + k_2AR, \\ \frac{\partial R}{\partial t} &= -k_{-1}IR + k_{1a}A + k_{-2}IR^* - k_2AR.\end{aligned}\quad (S1)$$

The rate constants are denoted as k_{-A} , k_A , k_{-I} , k'_I , k_{-2} , k_2 , k_{-1} , k_{1a} , k_{-2} and k_2 . The diffusion coefficient of the inhibitor I in the cytosolic region is represented by D . Note that, by the first and the second terms in the RHS of the fourth equation, the activator A and the inactivator I produce and degrade the inactive state of the response element R , respectively, which contribute to the amplification of the output signal R^* (5, 6). The capability of the system to show the spatial FCD in a static spatially-graded stimulus (5, 6) can be

understood by the spatial FCD symmetry of the model; at the steady state, i.e., $\frac{\partial A}{\partial t} = \frac{\partial I}{\partial t} = \frac{\partial R^*}{\partial t} = \frac{\partial R}{\partial t} = 0$, the solutions of Eqs. S1 are invariant under a scale transformation

$$(A, I, R^*, R, S) \rightarrow (pA, pI, R^*, R, pS) \quad (p > 0). \quad (S2)$$

However, without assuming the steady state, the scale invariance does not hold, meaning that the system does not show the temporal FCD property. Another model proposed by the authors combines the similar circuit to Eqs. S1 with an amplification module consisting of new variables, T and T_{in} (Fig. 3B in (6)):

$$\begin{aligned} \frac{\partial A}{\partial t} &= -k_{-A}A + k_A S, \\ \frac{\partial I}{\partial t} &= -k_{-I}I + k'_I S + D \nabla^2 I, \\ \frac{\partial R^*}{\partial t} &= -k_{-R}IR^* + k_R A(R_{tot} - R^*), \\ \frac{\partial T}{\partial t} &= k_T \frac{R^* T_{in}}{K_T + T_{in}} - k_\rho T, \\ \frac{\partial T_{in}}{\partial t} &= -k_T \frac{R^* T_{in}}{K_T + T_{in}} + k_\rho T + \sigma + k_\sigma T - \gamma_\sigma T_{in}, \end{aligned} \quad (S3)$$

where k_{-A} , k_A , k_{-I} , k'_I , k_{-R} , k_R , k_T , k_ρ , k_σ , K_T and γ_σ are rate constants. D and σ are the diffusion coefficient and the rate of constant supply of T_{in} , respectively. The total amount of the response elements (R_{tot}) is conserved. In addition to a feedforward circuit described by the first three equations, the fourth and fifth equations compose an amplification module based on a positive feedback loop, which locates at the downstream of the feedforward circuit (6). Although the system shows higher amplification of the input signal S (6), the system (Eqs. S3) shows essentially the same behavior as the previous one (Eqs. S2) from the point of view of the response rescaling. Namely, the equations are scale invariant upon a scale transformation,

$$(A, I, R^*, T, T_{in}, S) \rightarrow (pA, pI, R^*, T, T_{in}, pS) \quad (p > 0) \quad (S4),$$

only when the system is in the steady state. Thus, the temporal FCD is not achieved. However, the system shows the temporal FCD if we assume the kinetics of the third equation is sufficiently fast. In this case, the third equation becomes an algebraic equation as

$$R^* = \frac{k_A A}{k_A A + k_{-R} I} R_{tot}. \quad (S5)$$

Then, the system is now invariant to the scale transformation (Eqs. S4) without assuming the steady state and therefore shows both spatial and temporal FCDs.

Following this scheme, Wang et al. (7) have proposed a model in which the upstream module is the same as the first three equations in Eqs. S3 while the downstream amplification module is replaced by another one. Hence, the same logic as used in Eqs. S3 applies to their model; It satisfies the spatial FCD

symmetry without modification and, by assuming fast kinetics of one variable, it can be modified to achieve both symmetries.

(ii) A balanced inactivation model (8)

Levine et al. have proposed a LEGI-based model which, instead of assuming downstream amplification module as in Eqs. S3, introduces a hypothetical mutual inhibition between chemical components to describe amplification and adaptation (8). The governing equations are

$$\frac{\partial A}{\partial t} = k_a S - k_{-a} A - k_i A B_m \text{ at the membrane,}$$

$$\frac{\partial B_m}{\partial t} = k_b B - k_{-b} B_m - k_i A B_m \text{ at the membrane, and}$$

$$\frac{\partial B}{\partial t} = D \nabla^2 B \text{ in the cytosol (S6),}$$

with a boundary condition

$$D \frac{\partial B}{\partial n} = k_a S - k_b B,$$

where the derivative is the outward pointing normal derivative of the cytosolic component B . The rate constants are represented by k_a , k_{-a} , k_i , k_b and k_{-b} , respectively. D is the diffusion coefficient of the cytosolic component B . Due to the mutual inhibition term ($k_i A B_m$) in the first and second equations, the system does not show any scale invariance upon scale change in the input stimulus, i.e., $S \rightarrow pS$. As a result, the system shows neither the temporal FCD (Fig. 1 in (8)) nor the spatial FCD (in fact, the output level A in the steady state does not show perfect adaptation and depends on the absolute level of the input stimulus S as shown analytically in (8)).

(iii) Ultrasensitive LEGI model (5)

An alternative LEGI-based model has been proposed by Nakajima et al (5) to describe the responses in traveling wave stimuli. The governing equations are

$$\frac{\partial A}{\partial t} = k_a S - \gamma_a A,$$

$$\frac{\partial I}{\partial t} = k_i S - \gamma_i I + D \nabla^2 I,$$

$$\frac{\partial R}{\partial t} = A k_A \frac{R_{tot} - R}{K_A + (R_{tot} - R)} - I k_I \frac{R}{K_I + R},$$

where k_a , γ_a , k_i , γ_i , k_A , K_A , k_I and K_I are rate constants. D is the diffusion coefficient of the inhibitor I . This model has essentially the same upstream module as the model (S3), but the output signal R is now

regulated by the functions of Michaelis-Menten form, which is critical for the highly asymmetric response to spatially-symmetric traveling wave stimuli (5). In the same way as the previous model (Eqs. S3), this model satisfies the spatial FCD symmetry under the transformation,

$$(A, I, R, S) \rightarrow (pA, pI, R, pS) \quad (p > 0) \quad (S7).$$

This explains the rescaled response to a gradient stimulus of the model (5).

A possible molecular mechanism for the nonlinear activation function

In the scale-invariant LEGI model (Eqs. 1 in the main text), we adopted a nonlinear function $S^n/(S^n + (KB)^n)$ in which inhibitor B suppresses activator A by lowering the sensitivity to input S , not by degrading activator A directly. Below, we show how the sensitivity control can emerge in a biochemical network. Let us introduce a path inhibition model as follows:

$$\begin{aligned} \frac{\partial M}{\partial t} &= k_m S - k_{-m} B M \\ \frac{\partial A}{\partial t} &= k_a \frac{M^n}{M^n + K^n} - k_{-a} A, \\ \frac{\partial B}{\partial t} &= k_b S - k_{-b} B + D(\langle B \rangle - B), \end{aligned}$$

where k_m and k_{-m} represent the rate constants of the equation for M and the other parameters and variables are the same as in Eqs. 1. In this model, a signaling component M mediates excitatory regulation from the input S to the activator A , and the inhibitor B suppresses the mediator M instead of the activator signal directly (hence it is called a ‘path inhibition’ model). When the kinetics of M is fast, the mediator level M is approximated by S/B (Here we assume $k_m/k_{-m} = 1$ for simplicity). By substituting $M = S/B$ into the equation for A , we obtain the nonlinear sensitivity control function. The resultant model is equivalent to the scale-invariant LEGI model (Eqs. 1).

References

1. Parent, C.A., and P.N. Devreotes. 1999. A Cell 's Sense of Direction. *Science* (80-.). 284: 765–770.
2. Goentoro, L., O. Shoval, M.W. Kirschner, and U. Alon. 2009. The Incoherent Feedforward Loop Can Provide Fold-Change Detection in Gene Regulation. *Mol. Cell*. 36: 894–899.
3. Shoval, O., L. Goentoro, Y. Hart, A. Mayo, E. Sontag, and U. Alon. 2010. Fold-change detection and scalar symmetry of sensory input fields. *Proc. Natl. Acad. Sci. U. S. A.* 107: 15995–16000.
4. Adler, M., A. Mayo, and U. Alon. 2014. Logarithmic and Power Law Input-Output Relations in Sensory Systems with Fold-Change Detection. *PLoS Comput. Biol.* 10: e1003781.
5. Nakajima, A., S. Ishihara, D. Imoto, and S. Sawai. 2014. Rectified directional sensing in long-range cell migration. *Nat. Commun.* 5: 1–14.

6. Levchenko, A., and P.A. Iglesias. 2002. Models of eukaryotic gradient sensing: application to chemotaxis of amoebae and neutrophils. *Biophys. J.* 82: 50–63.
7. Wang, C.J., A. Bergmann, B. Lin, K. Kim, and A. Levchenko. 2012. Diverse sensitivity thresholds in dynamic signaling responses by social amoebae. *Sci. Signal.* 5: ra17.
8. Levine, H., D.A. Kessler, and W.-J. Rappel. 2006. Directional sensing in eukaryotic chemotaxis: a balanced inactivation model. *Proc. Natl. Acad. Sci. U. S. A.* 103: 9761–9766.